# Uncovering the critical soil moisture thresholds of plant water stress for European ecosystems

**Journal Article**

**Author(s):**
Fu, Zheng; Ciais, Philippe; Makowski, David; Bastos, Ana; Stoy, Paul C.; Ibrom, Andreas; Knohl, Alexander; Migliavacca, Mirco; Cuntz, Matthias; Šigut, Ladislav; Peichl, Matthias; Loustau, Denis; El-Madany, Tarek S.; Buchmann, Nina (iD); Gharun, Mana; Janssens, Ivan; Markwitz, Christian; Grünwald, Thomas; Rebmann, Corinna; Mölder, Meelis; Varlagin, Andrej; Mammarella, Ivan; Kolari, Pasi; Bernhofer, Christian; Heliasz, Michal; Vincke, Caroline; Pitacco, Andrea; Cremonese, Edoardo; Foltýnová, Lenka; Wigneron, Jean-Pierre

**DTU Library**

# Uncovering the critical soil moisture thresholds of plant water stress for European ecosystems

**Fu, Zheng; Ciais, Philippe; Makowski, David; Bastos, Ana; Stoy, Paul C.; Ibrom, Andreas; Knohl, Alexander; Migliavacca, Mirco; Cuntz, Matthias; Šigut, Ladislav**

*Total number of authors:*
30

*Citation (APA):*
Fu, Z., Ciais, P., Makowski, D., Bastos, A., Stoy, P. C., Ibrom, A., Knohl, A., Migliavacca, M., Cuntz, M., Šigut, L., Peichl, M., Loustau, D., ElMadany, T. S., Buchmann, N., Gharun, M., Janssens, I., Markwitz, C., Grünwald, T., Rebmann, C., ... Wigneron, JP. (2022). Uncovering the critical soil moisture thresholds of plant water stress for European ecosystems. *Global Change Biology*, *28*(6), 2111-2123. https://doi.org/10.1111/gcb.16050

1

2 DR. ZHENG  FU (Orcid ID : 0000-0001-7627-8824)

3 DR. ANA  BASTOS (Orcid ID : 0000-0002-7368-7806)

4 DR. LADISLAV  ŠIGUT (Orcid ID : 0000-0003-1951-4100)

5 DR. MATTHIAS  PEICHL (Orcid ID : 0000-0002-9940-5846)

6 DR. TAREK S. EL-MADANY (Orcid ID : 0000-0002-0726-7141)

7

8

10

11

12

**Uncovering the critical soil moisture thresholds of plant water stress for**

**European ecosystems**

15

18

19 Zheng Fu[1*], Philippe Ciais[1], David Makowski[2], Ana Bastos[3], Paul C. Stoy[4], Andreas Ibrom[5],

20 Alexander Knohl[6], Mirco Migliavacca[3], Matthias Cuntz[7], Ladislav Šigut[8], Matthias Peichl[9],

21 Denis Loustau[10], Tarek S. El-Madany[3], Nina Buchmann[11], Mana Gharun[11], Ivan Janssens[12],

22 Christian Markwitz[6], Thomas Grünwald[13], Corinna Rebmann[14], Meelis Mölder[15], Andrej

23 Varlagin[16], Ivan Mammarella[17], Pasi Kolari[17], Christian Bernhofer[13], Michal Heliasz[18],

24 Caroline Vincke[19], Andrea Pitacco[20], Edoardo Cremonese[21], Lenka Foltýnová[8], Jean-Pierre

25 Wigneron[10]

26

27    Zheng Fu: https://orcid.org/0000-0001-7627-8824

28    Philippe Ciais: https://orcid.org/0000-0001-8560-4943

29    Ana Bastos: https://orcid.org/0000-0002-7368-7806

30    Paul C. Stoy: https://orcid.org/0000-0002-6053-6232

31    Andreas Ibrom: https://orcid.org/0000-0002-1341-921X

32    Alexander Knohl: https://orcid.org/0000-0002-7615-8870

33    Mirco Migliavacca: https://orcid.org/0000-0003-3546-8407

34    Matthias Cuntz: https://orcid.org/0000-0002-5966-1829

35    Ladislav Šigut: https://orcid.org/0000-0003-1951-4100

36    Matthias Peichl: https://orcid.org/0000-0002-9940-5846

37    Tarek S. El-Madany: https://orcid.org/0000-0002-0726-7141

38    Nina Buchmann: https://orcid.org/0000-0003-0826-2980

39    Mana Gharun: https://orcid.org/0000-0003-0337-7367

40    Ivan Janssens: https://orcid.org/0000-0002-5705-1787

41    Thomas Grünwald: https://orcid.org/0000-0003-2263-0073

42    Corinna Rebmann: https://orcid.org/0000-0002-8665-0375

43    Andrej Varlagin: https://orcid.org/0000-0002-2549-5236

44    Ivan Mammarella: https://orcid.org/0000-0002-8516-3356

45    Christian Bernhofer: https://orcid.org/0000-0003-1061-3073

46    Michal Heliasz: https://orcid.org/0000-0003-2635-9604

47    Andrea Pitacco: https://orcid.org/0000-0002-7260-6242

48    Jean-Pierre Wigneron: https://orcid.org/0000-0001-5345-3618

49

50    [1] Laboratoire des Sciences du Climat et de l'Environnement, LSCE/IPSL, CEA-CNRS-UVSQ,

51    Université Paris-Saclay, Gif-sur-Yvette, 91191, France

52    [2] Unit Applied mathematics and computer science (UMR 518) INRAE AgroParisTech

53    Université Paris-Saclay, Paris, France

54 [3] Department Biogeochemical Integration, Max Planck Institute for Biogeochemistry, D-

55 07745 Jena, Germany

56 [4] Department of Biological Systems Engineering, University of Wisconsin – Madison, USA

57 [5] Technical University of Denmark, Department of Environmental Engineering, Lyngby,

58 Denmark

59 [6] University of Goettingen, Büsgenweg 2, 37077 Göttingen, Germany

60 [7] Université de Lorraine, AgroParisTech, INRAE, UMR Silva, 54000 Nancy, France

61 [8] Global Change Research Institute of the Czech Academy of Sciences, Bělidla 986/4a, CZ-

62 60300 Brno, Czech Republic

63 [9] Department of Forest Ecology and Management, Swedish University of Agricultural

64 Sciences, Skogsmarksgränd, 90183 Umeå, Sweden

65 [10] ISPA, Bordeaux Sciences Agro, INRAE, F-33140, Villenave d'Ornon, France

66 [11] Department of Environmental Systems Science, ETH Zurich, Universitaetstr. 2, 8092

67 Zurich, Switzerland

68 [12] Center of Excellence Global Change Ecology, Department of Biology, University of

69 Antwerp, Universiteitsplein 1, Wilrijk, 2610 Belgium

70 [13] Faculty of Environmental Sciences, Institute of Hydrology and Meteorology, Technische

71 Universität Dresden, 01062, Germany

72 [14] Department Computational Hydrosystems, Helmholtz Centre for Environmental Research –

73 UFZ

74 [15] Department of Physical Geography and Ecosystem Science, Lund University, Sölvegatan

75 12, SE-223 62 Lund, Sweden

76 [16] A.N. Severtsov Institute of Ecology and Evolution, Russian Academy of Sciences, 119071,

77 Leninsky pr.33, Moscow, Russia

78 [17] Institute for Atmospheric and Earth System Research/Physics, Faculty of Science,

79 University of Helsinki, Helsinki, Finland

80 [18] Centre for Environmental and Climate Research, Lund University, Lund, Sweden

81 [19] Earth and Life Institute - Environmental Sciences, Université catholique de Louvain

82   [20] University of Padova, DAFNAE, Viale dell'Università 16, I-35020 Legnaro, Italy

83   [21] Climate Change Unit, Environmental Protection Agency of Aosta Valley, Italy

84

85   *Correspondence to: zheng.fu@lsce.ipsl.fr

86

87 **Abstract**

88 Understanding the critical soil moisture (SM) threshold ($\theta_{crit}$) of plant water stress and land

89 surface energy partitioning is a basis to evaluate drought impacts and improve models for

90 predicting future ecosystem condition and climate. Quantifying the $\theta_{crit}$ across biomes and

91 climates is challenging because observations of surface energy fluxes and SM remain sparse.

92 Here, we used the latest database of eddy covariance measurements to estimate $\theta_{crit}$ across

93 Europe by evaluating evaporative fraction (EF)-SM relationships and investigating the

94 covariance between vapor pressure deficit (VPD) and gross primary production (GPP) during

95 SM dry-down periods. We found that the $\theta_{crit}$ and soil matric potential threshold in Europe are

96 16.5% and −0.7 MPa, respectively. Surface energy partitioning characteristics varied among

97 different vegetation types; EF in savannas had the highest sensitivities to SM in water-limited

98 stage, and the lowest in forests. The sign of the covariance between daily VPD and GPP

99 consistently changed from positive to negative during dry-down across all sites when EF

100 shifted from relatively high to low values. This sign of the covariance changed after longer

101 period of SM decline in forests than in grasslands and savannas. Estimated $\theta_{crit}$ from the VPD-

102 GPP covariance method match well with the EF-SM method, showing this covariance method

103 can be used to detect the $\theta_{crit}$. We further found that soil texture dominates the spatial

104 variability of $\theta_{crit}$ while shortwave radiation and VPD are the major drivers in determining the

105 spatial pattern of EF sensitivities. Our results highlight for the first time that the sign change

106 of the covariance between daily VPD and GPP can be used as an indicator of how ecosystems

107 transition from energy to SM limitation. We also characterized the corresponding $\theta_{crit}$ and its

108 drivers across diverse ecosystems in Europe, an essential variable to improve the

109 representation of water stress in land surface models.

110

111 **Keywords**: critical soil moisture threshold, surface energy partitioning, vapor pressure deficit,

112 evaporative          fraction,          gross          primary          production,          drought,          Europe

## 1. Introduction

The critical soil moisture (SM) threshold of plant water stress is the point when evapotranspiration starts to decrease due to the SM deficit (Feldman *et al.*, 2019, Seneviratne *et al.*, 2010). Below this threshold, exhaustion of SM leads to reduced evapotranspiration and increased partitioning towards sensible heat flux due to higher surface temperatures that lead to drier air and an increase in the vapor pressure deficit (VPD), which impairs important ecosystem functions like carbon dioxide uptake (Betts, 2004, Gentine *et al.*, 2019, Granier *et al.*, 2007, Seneviratne *et al.*, 2010). SM therefore plays a crucial role in partitioning of available between latent and sensible heat fluxes from the land surface (Schwingshackl *et al.*, 2017). This energy partitioning determines local climate and influences the terrestrial component of land-atmosphere coupling (Santanello Jr *et al.*, 2018). Thus, it is imperative to quantify the critical SM thresholds ($\theta_{crit}$) of plant water stress and surface energy partitioning characteristics for evaluating the drought impacts on ecosystem function and improving models to predict future climate accurately.

The evaporative fraction (EF) is the ratio of latent heat flux to the sum of latent and sensible heat fluxes, and EF-SM relationships are commonly used to quantify $\theta_{crit}$ and surface energy partitioning characteristics (Budyko, 1974, Koster *et al.*, 2009, Seneviratne *et al.*, 2010). SM directly limits evapotranspiration under SM-limited conditions, which increase surface temperature at a given level of net radiation, driving a positive land-atmosphere climate feedback (Betts, 2004, Gentine *et al.*, 2019, Seneviratne *et al.*, 2010). At higher SM availability, the system is considered energy limited as more moisture does not necessarily lead to greater evapotranspiration, and the strength of the water, carbon, and energy cycle coupling is subdued (Feldman *et al.*, 2019, Pendergrass *et al.*, 2020). Evapotranspiration is at or near its potential value where net radiation and atmospheric resistance are instead limiting. This EF-SM framework is well established (Fig. 1) but quantifying the $\theta_{crit}$ that determines the transition from energy to water-limited regimes across biomes and climates is challenging because surface energy fluxes and SM observations remain sparse (Baldocchi *et al.*, 2004,

140  Budyko, 1974, Feldman *et al.*, 2019, Koster *et al.*, 2009). The extreme drought events that

141  help quantify $\theta_{crit}$ are, by definition, rare, and often require long observational time series.

142  Attempts have been made to characterize these different evapotranspiration regimes at

143  sub-monthly scales using satellite greenness data and air temperature globally (Zscheischler *et*

144  *al.*, 2015), for North America (Short Gianotti *et al.*, 2019), and on weekly scales for Africa

145  using satellite remote sensing data of the diurnal amplitude of the land surface temperature

146  and surface soil moisture (Feldman *et al.*, 2019). These studies did not investigate the role of

147  VPD, but recently, both observations and models showed that VPD increases tend to reduce

148  gross primary production (GPP) across a large range of SM conditions, whereas the reduction

149  of SM only reduces GPP below a critical SM threshold (Green *et al.*, 2019, Grossiord *et al.*,

150  2020, Kimm *et al.*, 2020). GPP and evapotranspiration are tightly coupled on short time

151  scales (Gentine *et al.*, 2019), and we argue that the sign of the covariance between daily VPD

152  and GPP can be an indicator of the relative strength between the water and energy limitation

153  on ecosystem function. This is because VPD combines the effects of both water and enthalpy

154  (via temperature) on GPP (Grossiord *et al.*, 2020, Kimm *et al.*, 2020, Novick *et al.*, 2016).

155  GPP is positively related to radiation under energy-limited regimes (Fig. 1), and positively

156  correlated with SM under water-limited regimes (Gentine *et al.*, 2019, Seneviratne *et al.*,

157  2010). However, it is unknown if the sign change of covariance between daily VPD and GPP

158  is also an effective metric to a describe surface energy partitioning characteristics between

159  water- and energy-limited regimes, and *vice versa*.

160  The dry-down periods following rainfall, i.e., long periods without rainfalls when soil

161  moisture decreases (Akbar *et al.*, 2018, Feldman *et al.*, 2018, Feldman *et al.*, 2019), provide a

162  natural experiment for us to evaluate the EF-SM relationships and investigate how the sign of

163  the covariance between daily VPD and GPP changes as SM declines and ecosystems shift

164  from energy to water-limited states. During the course of a dry-down, an ecosystem with $\theta_{crit}$

165  will transition from a regime during which higher VPD is driven by incoming radiation which

166  increases GPP, to another regime where SM reductions increase VPD but reduce GPP. During

167  a SM dry-down, there is generally an initial period of GPP increase due to available SM after

168    rainfall if the ecosystem is already water limited before the dry-down counting started, and is

169    followed by a decline (Fig. 1); but VPD keeps increasing if the incoming solar radiation

170    (RAD) remains stable, e.g., in the presence of anticyclonic conditions (Feldman *et al.*, 2020).

171    During the initial increasing GPP period, energy-limitation (e.g., photosynthetically active

172    radiation or temperature) is the major driver of GPP while SM becomes a key limiting factor

173    during the following GPP decreasing stage (Seneviratne *et al.*, 2010). However, the

174    relationships between VPD and GPP in these two different stages may be different. We

175    hypothesize that the covariance between daily VPD and GPP can be used to detect these two

176    regimes during dry-downs, i.e., one regime with energy limiting conditions (positive

177    covariance) and one regime with water limiting conditions (negative covariance).

178        During a dry-down, EF first remains constant but then decreases when SM becomes

179    lower than a given threshold (Fig. 1). The EF–SM relationship is characterized by a transition

180    point in SM separating the water and energy-limited regimes (Koster *et al.*, 2009, Seneviratne

181    *et al.*, 2010). There is limited opportunity to test the appearance of SM limitations during dry

182    episodes across a wide diversity of biomes and climates because EF–SM relationships are

183    infrequently characterized due to the challenge of directly measuring surface energy fluxes

184    and SM across sites (Baldocchi *et al.*, 2004, Budyko, 1974, Feldman *et al.*, 2019, Koster *et al.*,

185    2009). To our knowledge, there is no observation-based assessment of the transition point of

186    SM between demand and soil water supply limitation across Europe. Even less is known

187    about the controlling factors and mechanisms in determining the $\theta_{crit}$ across diverse

188    ecosystems. Climate models, on the other hand, rely on a parametric representation of SM–

189    evaporation relationships to describe associations between water and energy cycles and

190    predict future climate. However, due to difficulty in observing EF at large scales to constrain

191    model results, and the lack of model simulation output at daily or hourly time steps, these

192    relationships take different forms across climate models which contribute to divergences and

193    uncertainty in making climate projections (Dirmeyer *et al.*, 2006, Feldman *et al.*, 2019,

194    Schwingshackl *et al.*, 2017).

195      The recently released ICOS (Integrated Carbon Observation System network of eddy

196    covariance observations)(Centre, 2019) dataset with continuously measured $CO_2$, water vapor,

197    and energy fluxes in Europe allows more direct observations of EF–SM relationships over

198    various biomes and climates. Further, this dense network provides a unique opportunity to

199    evaluate EF–SM relationships and change in the covariance between VPD and GPP during

200    dry-downs. In recent years, Europe has experienced a series of extreme summer drought and

201    heat events (e.g., 2003, 2010, 2015 and 2018), each characterized by record-breaking climate

202    anomalies and extensive dry-down periods (Bastos *et al.*, 2020a, Bastos *et al.*, 2020b, Fu *et*

203    *al.*, 2020). We can thus investigate the surface energy partitioning-SM relationship during

204    these dry-downs (episodes with no rain for several consecutive days (Fig. 1)) where SM

205    shows a short term rise after rain and then decreases until the next rain event. There were

206    many 'dry-down' periods with no rain in Europe in recent years that can be used to detect the

207    critical moisture value at the onset of water stress.

208      Focusing on SM dry-downs, this study uses the latest eddy covariance measurements

209    from ICOS to quantify $\theta_{crit}$ across Europe and test the hypothesis that the sign change of

210    covariance between daily VPD and GPP can be used to detect $\theta_{crit}$. By evaluating the EF-SM

211    relationships, we first quantify $\theta_{crit}$ values and the EF sensitivity to SM in the water-limited

212    regime. Then, we investigate the changes of covariance between daily VPD and GPP during

213    SM dry-downs and quantify $\theta_{crit}$ values with this second approach, which are compared with

214    the $\theta_{crit}$ from the first approach. Last, we explore what factors drive the spatial variability of

215    $\theta_{crit}$ and EF sensitivity to SM.

216

217    **2. Materials and Methods**

218    *2.1 Datasets*

219    We used half-hourly SM, VPD, GPP, precipitation, latent heat flux, sensible heat flux and

220    incoming shortwave radiation from the recently released ICOS (Integrated Carbon

221    Observation System) dataset (Centre, 2019). ICOS includes 52 eddy covariance sites in

222    Europe with energy, water, carbon fluxes and meteorological data, which were processed

223    following a consistent and uniform processing pipeline (Pastorello *et al.*, 2020). We selected

224    31 sites with measurements for all above variables, including 22 forests, 5 grasslands, 3

225    savannas and 1 shrubland (Table S1). Savanna sites include both trees and grasses and in our

226    case are found in Mediterranean climate zones (El-Madany *et al.*, 2020, Luo *et al.*, 2018, Luo

227    *et al.*, 2020). Croplands were excluded due to the effect of management on the seasonal

228    timing of ecosystem fluxes, both from crop rotations and from the varying timing of planting

229    and harvesting. Wetland sites were also removed because they have a high water table and

230    infrequently show soil moisture limitations.

231        SM was measured as volumetric soil water content (percentage) at different depths,

232    varying across sites. Surface SM (SM_1: 0-5 cm) was measured at all sites and some sites

233    also provided deeper SM measurements (e.g., SM_2: 5-20 cm; SM_3: 20-60 cm). We mainly

234    used the surface SM observations but deeper SM measurements were also used when

235    available. GPP estimates from the night-time partitioning method were used for the analysis

236    (Reichstein *et al.*, 2005). Data were quality controlled so that only measured and good-quality

237    gap filled data (QC = 0 or 1) were used. Daytime half-hourly data (9 am to 16 pm local

238    standard time) were averaged to daily values while SM values were averaged over the full day.

239        Measured soil texture, mean annual precipitation, summer average of VPD, incoming

240    shortwave radiation and wind speed data at each site were also used to understand the drivers

241    in determining the spatial variability of $\theta_{crit}$ and EF sensitivity to SM in water-limited stage.

242

243    ### *2.2 Soil moisture dry-down identification*

244    Dry-downs following rainfall are episodes with no rain for several consecutive days during

245    which SM shows a short term 'pulse' rise after rain and then decays until the next rain event.

246    A dry-down is retained for our analysis when SM decreases consecutively for at least 10 days

247    after rainfall (Akbar *et al.*, 2018, Feldman *et al.*, 2018, McColl *et al.*, 2017, Shellito *et al.*,

248    2018). Days with intermittent rainfall are excluded. We focused on the soil dry-downs during

249    the summer (June−July−August) season for all available site-years. This resulted in 428 dry-

250    down events that form the basis of our study.

251

### 2.3 Critical SM threshold and evaporative fraction sensitivity to SM estimation

We calculated the daily evaporative fraction (EF) as the ratio of observed latent heat flux to the sum of latent and sensible heat fluxes during each soil dry-down. Then, we characterized the EF-SM relationship at each site using all available soil dry-downs, from a regression between these two variables with a linear-plus-plateau model:

$$EF = \begin{cases} a + b(SM - c) & if\ SM < \theta_{crit} \\ a & if\ SM \geq \theta_{crit} \end{cases}$$

where $a$ is the maximum value of EF in absence of SM stress (energy-limited stage), $b$ represents the slope of the linear increase phase (water-limited stage), and $c$ is the critical SM threshold. These three parameters were simultaneously estimated by least squares fit with the R software package 'nlstools' (Baty *et al.*, 2015) for each site, leading to site-specific estimated values of peak EF, slope and $\theta_{crit}$. $\theta_{crit}$ is the breakpoint until which EF increases linearly as a function of SM (Figs. 1 and S1). The slope represents the EF sensitivity to SM in the water‑limited regime, indicating the magnitude of EF increase for each additional 1% change in SM when SM is below its breakpoint. The plateau is the maximum EF value reached when SM exceeds its threshold. The time spent in the water‑limited stage was computed as the ratio of the number of days with SM<threshold divided by the total duration of the dry down as in Feldman *et al.* (2019). SM threshold values were converted to soil matric potentials using soil retention curves and soil texture data (Table S1) (Gourlez de la Motte *et al.*, 2020, Granier *et al.*, 2007, Marthews *et al.*, 2014).

There were 23, 16 and 12 sites with the critical SM threshold estimates based on the first (SM_1), second (SM_2), and third (SM_3) soil water content measurement depth (Figs. S1-3), respectively. For the rest of sites, it was not possible to estimate a SM threshold using the EF-SM relationship because samples were too infrequent, deep SM measurements were missing, or there were no thresholds.

### 2. 4 Covariance between daily VPD and GPP during dry-down

We also calculated the covariance between daily VPD and GPP across nine-day moving

279    windows during the dry-down (e.g., 1-9 days; 2-10 days; 3-11 days…). A positive covariance

280    indicates that higher VPD is associated with increases of GPP (which we term 'radiation

281    effects') while a negative covariance indicates that water stress limits GPP, i.e., with a higher

282    VPD caused by dryer soils results in a lower GPP. Here, we excluded some short dry-downs

283    because their covariances during the dry-down are all positive or negative, suggesting the

284    entire dry-down period is under energy-limited or water-limited stage. We only chose the

285    long soil dry-downs with at least 15 days (with at least 7 covariance values) and their

286    covariances must include both positive and negative values to see if the change of covariance

287    signs corresponds to the ecosystem transition from energy-limited into water-limited regime.

288        The evolution of covariance with moving window days during the dry-down periods

289    allowed us to evaluate the joint variability of daily VPD and GPP change. Across all soil dry-

290    downs, the median value of the VPD-GPP covariance was calculated for equal bins of 1 day

291    change to identify the timing when the sign of covariance will change. Similar to the

292    covariance, the average of SM during the moving window (e.g., 1-9 days; 2-10 days; 3-11

293    days…) were also calculated to detect the critical SM threshold when the sign of covariance

294    changes. The correlation of Pearson and Spearman and their associated test were performed to

295    compare the $\theta_{crit}$ values from this covariance method with the EF-SM method.

296

297    *2.5 Drivers of the spatial variability of critical SM thresholds and EF slopes*

298    We evaluated the relative importance of soil texture, mean annual precipitation, summer

299    average VPD, incoming shortwave radiation and wind speed in determining the spatial

300    variability of $\theta_{crit}$ and EF sensitivities to SM. We used a relative importance analysis approach

301    to quantify the relative contributions of each factor to the SM thresholds or EF slopes,

302    expressed as the Pearson correlation in a multiple linear regression (SM thresholds (or EF

303    slopes)= $b_0 + b_1 \times$ MAP + $b_2 \times$ Clay fraction + $b_3 \times$ VPD + $b_4 \times$ radiation + $b_5 \times$ wind + $\varepsilon$). $\varepsilon$

304    represented other drivers that were not considered but might contribute to the variability of

305    SM thresholds or EF slopes. The algorithm was implemented with the 'relaimpo' package in

306    R (Grömping, 2006), which is based on variance decomposition for multiple linear regression

307  models. The 'relaimpo' package provides six different methods for analyzing the relative

308  importance of each regressor in linear regression. We used 'LMG' to quantify the contribution

309  of different correlated regressors in a multiple linear regression (Huang *et al.*, 2018). The

310  LMG method estimates the relative importance (RI) of each variable by decomposing the sum

311  of squares into non-negative contributions shared by each variable, and the LMG values were

312  obtained by averaging the sequential sum of squares ($r^2$) for all possible orders. Finally, all RI

313  values were normalized (divided by $r^2$) to sum to 1. We also repeated this analysis using the

314  available energy (AE, the difference between net radiation and soil heat flux) instead of the

315  incoming shortwave radiation to evaluate the relative role of AE.

316

317  **3. Results**

318  *3.1 Surface energy partitioning characteristics and critical SM threshold of plant stress*

319  EF behavior during all dry-downs within each vegetation type is plotted together in Figure 2.

320  The general behavior is in line with that shown in Figure 1. Temperate grasslands and

321  Mediterranean savannas showed stronger EF–SM coupling (greater slope) at low soil

322  moisture values than boreal and temperate forests. The available energy is increasingly

323  partitioned towards sensible heat flux with decreasing SM during the water-limited regime.

324  The surface SM thresholds (using SM_1) is highly correlated with the SM thresholds

325  observed in deeper soil layers (using SM_2 and SM_3) (Fig. S4). As surface SM

326  measurements are available at all sites, we focused on surface SM thresholds. Across all sites,

327  we found that the critical SM threshold in Europe is 16.5 ± 7.5% (median ± SD, Fig. 3a).

328  Temperate grasslands (27.0 ± 10.6%) had higher SM thresholds than temperate forests (16.5

329  ± 5.5%) and Mediterranean savannas (13.0 ± 1.6%, Fig. 3c). We also found that the soil

330  matric potential threshold in savannas (−1.22 ± 0.21 MPa) is more negative than in forests

331  (−0.64 ± 0.45 MPa) and grasslands (−0.37 ± 0.49 MPa, Fig. 3c). Overall, we estimated that

332  the critical soil matric potential threshold across all sites in Europe is −0.71 ± 0.46 MPa (Fig.

333  3b).

334       The sensitivities (slopes) of EF to SM, time spent in water-limited stage, and the peak

335    EFs are different among vegetation types (Fig. 4). Across all sites, EF decreased by 0.03 per 1%

336    SM decrease (Fig. 4a). Savannas showed a higher sensitivity of EF to SM (slope $0.05 \pm 0.02$)

337    than forests (slope $0.03 \pm 0.02$). We further found that the time spent in water-limited stage in

338    savannas ($82.9 \pm 9.7\%$ of all dry-down durations) was nearly two times as long as in forests

339    ($44.0 \pm 24.1\%$); across all European sites, it was about $48.3 \pm 27.0\%$ of the dry-down period

340    duration (Fig. 4b). However, the peak EF in energy-limited stage in forests ($0.5 \pm 0.1$) tended

341    to be higher than in savannas ($0.4 \pm 0.1$, Fig. 4c).

342

343    *3.2 Covariance between daily VPD and GPP during SM dry-down*

344    As an alternative to the EF-SM relationships, the change in the sign of the covariance

345    between daily GPP and VPD during dry-down was used to detect the critical SM threshold.

346    To explore the dynamics of the VPD-GPP relationships during dry-down, we first illustrated

347    the changes in the covariance of daily GPP and VPD during a long soil moisture dry-down at

348    CH-Cha (grassland, Figs.5a, b), as well as the coincident changes in surface energy

349    partitioning–SM relationship (Fig. 5c). Both the original data and moving average data found

350    that daily GPP first increases but then decreases during the dry-down while daily VPD

351    increases steadily (Fig. 5a). The sign of covariance between daily VPD and GPP changed

352    from positive into negative around a SM threshold of 35% for this example (Fig. 5b). The

353    positive covariances suggested that positive radiation effects (VPD-radiation coupling) on

354    GPP are stronger while negative covariances showed that SM limiting effects on GPP are

355    stronger (VPD-SM coupling). The EF-SM relationship showed that the EF values remain

356    relatively high (about 0.75) at high SM (35-55%); however, under low SM (<35%), EF and

357    SM were positively related in the interval during which reduced SM lowers EF (Fig. 5c).

358    These observations are consistent with the notion that the ecosystem shifted from an energy-

359    limited regime to a water-limited regime during this dry-down such that the sign of

360    covariance between daily VPD and GPP was related to surface energy partitioning. Another

361    example in a forest site, DE-Hzd, yielded similar results (Fig. S5).

362    We also examined the covariance between daily VPD and GPP for all soil dry-downs

363    (Fig. 6). All covariances consistently changed their signs from positive to negative during the

364    dry-down (Fig. 6a). We found that the median values of covariances across all dry-downs

365    revealed that the breakpoint often occurs around the 4th moving window (the covariance is

366    calculated using 9-day moving window, e.g., 1-9 days; 2-10 days; 3-11 days…). The changed

367    covariance signs are also found in different vegetation types consistently (Figs. 6b-d). The

368    timing of the breakpoint in forests (5th moving window, Fig. 6b) is larger than in grasslands

369    (3rd moving window, Fig. 6c) and savannas (2nd moving window, Fig. 6d), suggesting that it

370    takes longer for the VPD-GPP covariance sign to change from positive to negative in forests

371    compared to grasslands and savannas. As the savanna sites have Mediterranean climate and

372    the peak growing season is mainly in spring (El-Madany *et al.*, 2020, Luo *et al.*, 2018, Luo *et*

373    *al.*, 2020), we performed the same analysis using both spring and summer and obtained

374    similar results that the breakpoint in savannas is reached in shorter time than in forests (Fig.

375    S6).

376    Combining the SM data for each dry-down (Figs. 6e-h), we then quantified the critical

377    SM thresholds when the VPD-GPP covariance sign change at each site. We found that the $\theta_{crit}$

378    estimated from the new covariance method match well with the EF-SM method (r=0.86, Figs.

379    6i-j). Compared with the $\theta_{crit}$ estimated from the EF-SM method, our results showed that the

380    VPD-GPP covariance method has potential to detect the critical moisture thresholds, although

381    the absolute magnitude of SM thresholds estimated from covariance method are a bit higher

382    than that of EF-SM methods (Figs. 6i-j).

383

384    *3.3 Drivers of the spatial variability of SM thresholds and EF slopes*

385    The multiple linear regression model showed that the five factors studied (mean annual

386    precipitation, clay fraction, summer VPD, incoming shortwave radiation and wind speed) can

387    explain 74% and 65% of the spatial variability of SM thresholds (Fig. 7a) and EF sensitivities

388    (Fig. 7b), respectively. However, the dominant predictors of the spatial variability of SM

389    thresholds and reduction rates of EF were different. For the spatial variability of SM

390    thresholds, soil texture was the most important factor, and its relative importance was 76%

391    comparing with the other four factors (Fig. 7a), and clay fraction alone explained 65% of the

392    variability across all sites. For the spatial variability of reduction rates of EF, climate factors,

393    such as incoming shortwave radiation and VPD, were the major drivers, with relative

394    importance up to 53% and 26%, respectively (Fig. 7b). The same analysis using the available

395    energy (AE, the difference between net radiation and soil heat flux) instead of the incoming

396    shortwave radiation obtained similar results (Fig. S7). AE played an important role in

397    determining both the spatial variability of $\theta_{crit}$ (17%) and EF sensitivities (52%, Fig. S7).

398

399    **4. Discussion**

400    Current water stress indicators typically hinge on the accuracy of evapotranspiration data, a

401    flux that is very difficult to measure globally and is often estimated with assumptions, thus

402    leading to high degrees of uncertainty (Wang & Dickinson, 2012). To our knowledge, we

403    demonstrate for the first time that the covariance between daily VPD and GPP changes its

404    sign from positive to negative during SM dry-downs as ecosystems transition from energy-

405    limited regimes to water-limited regimes. Our results suggest that the sign of covariance

406    between daily VPD and GPP can capture shifts in the surface energy partitioning

407    characteristics and therefore has potential to be a new indicator of ecosystem water stress. For

408    global remote sensing data products, it becomes possible to have reasonable GPP products,

409    e.g., based Near-Infrared Reflectance of vegetation ($NIR_V$) (Badgley et al., 2017), normalized

410    difference vegetation index (NDVI) (Myneni et al., 1997), enhanced vegetation index (EVI)

411    (Huete et al., 2002) and daily FLUXCOM data (Jung et al., 2017, Tramontana et al., 2016),

412    and VPD is computed from directly observed temperature and relative humidity, whereas

413    global evapotranspiration products differ between datasets and are arguably more uncertain

414    (Badgley et al., 2015, Bai & Liu, 2018). Our covariance method provides a new option and

415    an independent tool to quantify the critical SM threshold and detect surface energy

416    partitioning characteristics over large regions, which we hope will be helpful to uncover the

417    SM thresholds of plant water stress at regional and global scales. One advantage of the

418    covariance indicator is that, from a remote sensing perspective, spatially resolved VPD and

419    GPP products have much lower levels of uncertainty than evapotranspiration products.

420    Another is that the type of stress is directly related to GPP, i.e., carbon uptake, and not only

421    indicative for stomatal conductance and transpiration.

422    Although the critical SM thresholds estimated from VPD-GPP covariance method match

423    well with the EF-SM method, we found that the absolute magnitude of SM thresholds

424    estimated from the VPD-GPP covariance method are a bit higher than the EF-SM method

425    (Figs. 6i-j), which may result from two reasons. First, the covariance method calculated the

426    covariance and mean SM values using nine-day moving windows. The average values of SM

427    across the window could lead to the difference of SM thresholds between the VPD-GPP

428    covariance method and EF-SM method. Second, the eddy covariance evapotranspiration

429    analysis measures not only plant transpiration but also soil evaporation (though it is often

430    small) (Stoy *et al.*, 2019), which may also contribute to the differences found between

431    approaches. To get a more plant-related estimate of the critical SM threshold, the response of

432    plant functioning (GPP and transpiration) with atmospheric stress (VPD) under given soil

433    moisture conditions needs to be taken into account.

434    The timing when the sign of the covariance between VPD and GPP changes from

435    positive to negative varies across vegetation types. Forests need more time for the sign of this

436    relationship to change after rain events than grasslands and savannas, showing that there is a

437    longer time during which VPD-radiation coupling is stronger than VPD-SM coupling in

438    forests compared to grasslands and savannas during SM dry-downs. The water storage in soil

439    and plants after rainfall in forests can be larger than in grasslands because forests have deeper

440    roots and access to moisture in deeper soils (Chapin III *et al.*, 2011, Fan *et al.*, 2017). Forests

441    often have stronger resistance to drought than grasslands and savannas (Konings & Gentine,

442    2017, Martínez-Vilalta & Garcia-Forner, 2017, Teuling *et al.*, 2010), thus GPP rates are

443    maintained for a longer time after rainfall in forests.

444    The surface energy partitioning-SM relationship showed that grasslands and savannas

445    had stronger EF–SM coupling (slope) at low soil moisture values than that of forests (Figs. 2

446    and 4a). Grasslands have shallow roots and are more sensitive to SM decrease, leading to
447    abrupt drought, while forests have deep roots, access to deep soil water, and less sensitive to
448    surface soil moisture changes. The high sensitivity of EF to SM in water-limited periods in
449    grasslands and savannas will accelerate soil moisture depletion and quickly lead to large
450    water constraints on photosynthesis (El-Madany *et al.*, 2020, Luo *et al.*, 2018, Luo *et al.*,
451    2020). The low sensitivity of EF to SM in forests is in line with our findings from covariance
452    analysis that showed it takes longer for the VPD-GPP covariance sign to change from positive
453    to negative in forests compared to grasslands and savannas, further supported the strong
454    resistance of forests to drought (Konings & Gentine, 2017, Teuling *et al.*, 2010). We also
455    found that incoming shortwave radiation and VPD are the major drivers in determining the
456    spatial variability of EF sensitivity to SM, indicating that high radiation and VPD will
457    increase the sensitivity of EF to SM in water-limited stage. This will likely cause EF
458    sensitivity to increase in the future because increased exposure of plants to higher VPD from
459    warming and drier continental relative humidity is inevitable and widespread in future (Byrne
460    &  O'Gorman, 2018, Novick *et al.*, 2016).

461    Consistent with previous findings from satellite observations in Africa (Feldman et al.,
462    2019), our results showed that savannas spend more time in the water‐limited regime, but we
463    found that forests also spend almost 50% of the time in the water‐limited regime, suggesting
464    that European forest ecosystems are exposed to drought. This time fraction spent in the water‐
465    limited regime may further increase in future with anthropogenic warming (Naumann *et al.*,
466    2021), leading to greater drought damages in Europe. We also found that grasslands spend
467    more than 70% of the time in the energy‐limited regime because these grassland sites are
468    mainly located in the northern Europe, which are limited by energy due to the high latitudes
469    or altitudes. Under energy-limited stage, the peak EF in grasslands was up to 0.79 (Fig. 4c),
470    indicating that grasslands allocate more energy for evaporative cooling, which suppresses
471    surface heating (Teuling *et al.*, 2010).

472    Across all sites in Europe, our results showed that the critical SM threshold is 16.5% (Fig.
473    5), which is slightly higher than the value found in Africa (14%) using a different method

474     (Feldman *et al.*, 2019) and an oak–grass savanna (15%) and an annual grassland (15%) in US

475     (Baldocchi *et al.*, 2004). At the European sites, we found that soil texture is the most

476     important determining factor in controlling the spatial variability of SM thresholds (Fig. 7a),

477     which is in line with previous findings in Africa (Feldman *et al.*, 2019) and the US (Akbar *et*

478     *al.*, 2018), based on satellite data. We also converted the SM thresholds into soil matric

479     potentials, and found that the soil matric potential threshold in Europe is about −0.71 MPa.

480     The soil matric potential threshold in savannas is more negative than in forests and grasslands.

481     When we focused on the forest sites in Europe, we found that the soil matric potential

482     threshold is −0.64 MPa, which is very close from the -0.66 MPa value found by Granier *et al.*

483     (2007) across six forest ecosystems. We noted that the EF-SM relationship can be affected by

484     other factors, such as radiation and albedo (Haghighi *et al.*, 2018). While several other factors

485     limit evapotranspiration besides soil moisture and the linear dependency is a simple

486     approximation, recent studies have highlighted that this EF-SM framework provides a good

487     first-order representation of regimes of land–atmosphere coupling, both in models and

488     observations (e.g., Koster *et al.* (2004a); Koster *et al.* (2004b); Seneviratne *et al.* (2006);

489     Teuling *et al.* (2006)). Here we provided a comprehensive analysis across representative

490     European ecosystems.

491

## 5. Conclusions

493     Using a new database of flux tower observations across Europe, this study uncovered the

494     critical SM threshold and surface energy partitioning characteristics by evaluating EF-SM

495     relationships and examining the joint variability of daily VPD and GPP during SM dry-downs.

496     We carefully studied SM dry-downs to understand how ecosystems transition from energy-

497     limited regimes to water-limited regimes. EF-SM relationships quantified the critical SM and

498     soil matric potential thresholds in Europe are 16.5% and −0.7 MPa, respectively. Surface

499     energy partitioning characteristics varied among different vegetation types; EF in savannas

500     had the highest sensitivities to SM in water-limited stage while it was the lowest in forests.

501     We found the sign of covariance between daily VPD and GPP changed after a longer period

502    in forests than in grasslands and savannas. The critical SM thresholds estimated from the

503    VPD-GPP covariance method match well with that of EF-SM method, suggesting that this

504    sign of VPD-GPP covariance can be used to detect the SM threshold. We further found that

505    soil texture dominates the spatial variability of SM thresholds while incoming shortwave

506    radiation and VPD are the major drivers in determining the spatial pattern of EF sensitivities.

507    The revealed critical SM threshold and its drivers across diverse biomes and climates in

508    Europe will be beneficial to improve climate models with parametric representations of

509    drought stress. Our results highlighted, for the first time, the important role of the sign change

510    of covariance between daily VPD and GPP in monitoring the surface energy partitioning

511    characteristics and quantifying the critical SM threshold, which opens its generalized

512    application using daily GPP estimates and VPD, e.g., from remote sensing data. The new

513    covariance method demonstrated here provides a new option and an independent tool to

514    quantify critical SM threshold and surface energy partitioning, which can help solve the

515    current challenge in uncovering the SM threshold of plant water stress at regional and global

516    scales.

517

518    **Acknowledgements**

527

528    **Conflict of interest**

529    The authors declare no competing interests.

530

**Data availability**

531

The data that support the findings of this study are openly available in ICOS at

532

(https://doi.org/10.18160/YVR0-4898).

533

534    **References**

535    Akbar R, Gianotti DJS, Mccoll KA, Haghighi E, Salvucci GD, Entekhabi D (2018)

536        Estimation of landscape soil water losses from satellite observations of soil moisture.

537        Journal of Hydrometeorology, **19**, 871-889.

538    Badgley G, Field CB, Berry JA (2017) Canopy near-infrared reflectance and terrestrial

539        photosynthesis. Science advances, **3**, e1602244.

540    Badgley G, Fisher JB, Jiménez C, Tu KP, Vinukollu R (2015) On uncertainty in global

541        terrestrial evapotranspiration estimates from choice of input forcing datasets. Journal

542        of Hydrometeorology, **16**, 1449-1455.

543    Bai P, Liu X (2018) Intercomparison and evaluation of three global high-resolution

544        evapotranspiration products across China. Journal of hydrology, **566**, 743-755.

545    Baldocchi DD, Xu L, Kiang N (2004) How plant functional-type, weather, seasonal drought,

546        and soil physical properties alter water and energy fluxes of an oak–grass savanna

547        and an annual grassland. Agricultural and Forest Meteorology, **123**, 13-39.

548    Bastos A, Ciais P, Friedlingstein P *et al.* (2020a) Direct and seasonal legacy effects of the

549        2018 heat wave and drought on European ecosystem productivity. Science advances,

550        **6**, eaba2724.

551    Bastos A, Fu Z, Ciais P *et al.* (2020b) Impacts of extreme summers on European ecosystems:

552        a comparative analysis of 2003, 2010 and 2018. Philosophical Transactions of the

553        Royal Society B, **375**, 20190507.

554    Baty F, Ritz C, Charles S, Brutsche M, Flandrois J-P, Delignette-Muller M-L (2015) A

555        toolbox for nonlinear regression in R: the package nlstools. Journal of statistical

556        software, **66**, 1-21.

557    Betts AK (2004) Understanding hydrometeorology using global models. Bulletin of the

558        American Meteorological Society, **85**, 1673-1688.

559    Budyko MI (1974) *Climate and life*, Academic press.

560    Byrne MP, O'gorman PA (2018) Trends in continental temperature and humidity directly

561        linked to ocean warming. Proceedings of the National Academy of Sciences, **115**,

562        4863-4868.

563    Centre DTIET (2019) Drought-2018 ecosystem eddy covariance flux product in FLUXNET-

564        Archive format - release 2019-1. ICOS Carbon Portal. (doi:10.18160/PZDK-EF78).

565    Chapin Iii FS, Matson PA, Vitousek P (2011) *Principles of terrestrial ecosystem ecology*,

566        Springer Science & Business Media.

567    Dirmeyer PA, Koster RD, Guo Z (2006) Do global models properly represent the feedback

568        between land and atmosphere? Journal of Hydrometeorology, **7**, 1177-1198.

569    El-Madany TS, Carrara A, Martín MP *et al.* (2020) Drought and heatwave impacts on semi-

570        arid ecosystems' carbon fluxes along a precipitation gradient. Philosophical

571        Transactions of the Royal Society B, **375**, 20190519.

572    Fan Y, Miguez-Macho G, Jobbágy EG, Jackson RB, Otero-Casal C (2017) Hydrologic

573        regulation of plant rooting depth. Proceedings of the National Academy of Sciences,

574        **114**, 10572-10577.

575    Feldman AF, Gianotti DJS, Konings AG, Mccoll KA, Akbar R, Salvucci GD, Entekhabi D

576        (2018) Moisture pulse-reserve in the soil-plant continuum observed across biomes.

577        Nature plants, **4**, 1026-1033.

578    Feldman AF, Short Gianotti DJ, Trigo IF, Salvucci GD, Entekhabi D (2019) Satellite-based

579        assessment of land surface energy partitioning–soil moisture relationships and effects

580        of confounding variables. Water Resources Research, **55**, 10657-10677.

581    Feldman AF, Short Gianotti DJ, Trigo IF, Salvucci GD, Entekhabi D (2020) Land-

582        Atmosphere Drivers of Landscape-Scale Plant Water Content Loss. Geophysical

583        Research Letters, **47**, e2020GL090331.

584    Fu Z, Ciais P, Bastos A *et al.* (2020) Sensitivity of gross primary productivity to climatic

585        drivers during the summer drought of 2018 in Europe. Philos Trans R Soc Lond B

586        Biol Sci, **375**, 20190747.

587    Gentine P, Green JK, Guérin M, Humphrey V, Seneviratne SI, Zhang Y, Zhou S (2019)

588        Coupling between the terrestrial carbon and water cycles—a review. Environmental

589        Research Letters, **14**, 083003.

590    Gourlez De La Motte L, Beauclaire Q, Heinesch B *et al.* (2020) Non-stomatal processes

591        reduce gross primary productivity in temperate forest ecosystems during severe

592        edaphic drought. Philosophical Transactions of the Royal Society B, **375**, 20190527.

593    Granier A, Reichstein M, Bréda N *et al.* (2007) Evidence for soil water control on carbon and

594        water dynamics in European forests during the extremely dry year: 2003. Agricultural

595        and Forest Meteorology, **143**, 123-145.

596    Green JK, Seneviratne SI, Berg AM, Findell KL, Hagemann S, Lawrence DM, Gentine P

597        (2019) Large influence of soil moisture on long-term terrestrial carbon uptake. Nature,

598        **565**, 476-479.

599    Grömping U (2006) Relative importance for linear regression in R: the package relaimpo.

600        Journal of statistical software, **17**, 1-27.

601    Grossiord C, Buckley TN, Cernusak LA *et al.* (2020) Plant responses to rising vapor pressure

602        deficit. New Phytologist, **226**, 1550-1566.

603    Haghighi E, Short Gianotti DJ, Akbar R, Salvucci GD, Entekhabi D (2018) Soil and

604        atmospheric controls on the land surface energy balance: A generalized framework

605        for distinguishing moisture-limited and energy-limited evaporation regimes. Water

606        Resources Research, **54**, 1831-1851.

607    Huang K, Xia J, Wang Y *et al.* (2018) Enhanced peak growth of global vegetation and its key

608        mechanisms. Nat Ecol Evol, **2**, 1897-1905.

609    Huete A, Didan K, Miura T, Rodriguez EP, Gao X, Ferreira LG (2002) Overview of the

610        radiometric and biophysical performance of the MODIS vegetation indices. Remote

611        Sensing of Environment, **83**, 195-213.

612    Jung M, Reichstein M, Schwalm CR *et al.* (2017) Compensatory water effects link yearly

613        global land CO2 sink changes to temperature. Nature, **541**, 516-520.

614    Kimm H, Guan K, Gentine P *et al.* (2020) Redefining droughts for the U.S. Corn Belt: The

615              dominant role of atmospheric vapor pressure deficit over soil moisture in regulating

616              stomatal behavior of Maize and Soybean. Agricultural and Forest Meteorology, **287**,

617              107930.

618    Konings AG, Gentine P (2017) Global variations in ecosystem-scale isohydricity. Global

619              change biology, **23**, 891-905.

620    Koster R, Schubert S, Suarez M (2009) Analyzing the concurrence of meteorological

621              droughts and warm periods, with implications for the determination of evaporative

622              regime. Journal of Climate, **22**, 3331-3341.

623    Koster RD, Dirmeyer PA, Guo Z *et al.* (2004a) Regions of strong coupling between soil

624              moisture and precipitation. Science, **305**, 1138-1140.

625    Koster RD, Suarez MJ, Liu P *et al.* (2004b) Realistic initialization of land surface states:

626              Impacts on subseasonal forecast skill. Journal of Hydrometeorology, **5**, 1049-1063.

627    Luo Y, El-Madany TS, Filippa G *et al.* (2018) Using near-infrared-enabled digital repeat

628              photography to track structural and physiological phenology in Mediterranean tree–

629              grass ecosystems. Remote Sensing, **10**, 1293.

630    Luo Y, El-Madany T, Ma X *et al.* (2020) Nutrients and water availability constrain the

631              seasonality of vegetation activity in a Mediterranean ecosystem. Global change

632              biology, **26**, 4379-4400.

633    Marthews TR, Quesada CA, Galbraith DR, Malhi Y, Mullins CE, Hodnett MG, Dharssi I

634              (2014) High-resolution hydraulic parameter maps for surface soils in tropical South

635              America. Geoscientific Model Development, **7**, 711-723.

636    Martínez-Vilalta J, Garcia-Forner N (2017) Water potential regulation, stomatal behaviour

637              and hydraulic transport under drought: deconstructing the iso/anisohydric concept.

638              Plant, Cell & Environment, **40**, 962-976.

639    Mccoll KA, Wang W, Peng B *et al.* (2017) Global characterization of surface soil moisture

640              drydowns. Geophysical Research Letters, **44**, 3682-3690.

641     Myneni RB, Ramakrishna R, Nemani R, Running SW (1997) Estimation of global leaf area

642           index and absorbed PAR using radiative transfer models. IEEE Transactions on

643           Geoscience and remote sensing, **35**, 1380-1393.

644     Naumann G, Cammalleri C, Mentaschi L, Feyen L (2021) Increased economic drought

645           impacts in Europe with anthropogenic warming. Nature Climate Change, **11**, 485-491.

646     Novick KA, Ficklin DL, Stoy PC *et al.* (2016) The increasing importance of atmospheric

647           demand for ecosystem water and carbon fluxes. Nature Climate Change, **6**, 1023.

648     Pastorello G, Trotta C, Canfora E *et al.* (2020) The FLUXNET2015 dataset and the ONEFlux

649           processing pipeline for eddy covariance data. Scientific data, **7**, 1-27.

650     Pendergrass AG, Meehl GA, Pulwarty R *et al.* (2020) Flash droughts present a new challenge

651           for subseasonal-to-seasonal prediction. Nature Climate Change, **10**, 191-199.

652     Reichstein M, Falge E, Baldocchi D *et al.* (2005) On the separation of net ecosystem

653           exchange into assimilation and ecosystem respiration: review and improved algorithm.

654           Global change biology, **11**, 1424-1439.

655     Santanello Jr JA, Dirmeyer PA, Ferguson CR *et al.* (2018) Land–atmosphere interactions:

656           The LoCo perspective. Bulletin of the American Meteorological Society, **99**, 1253-

657           1272.

658     Schwingshackl C, Hirschi M, Seneviratne SI (2017) Quantifying spatiotemporal variations of

659           soil moisture control on surface energy balance and near-surface air temperature.

660           Journal of Climate, **30**, 7105-7124.

661     Seneviratne SI, Corti T, Davin EL *et al.* (2010) Investigating soil moisture–climate

662           interactions in a changing climate: A review. Earth-Science Reviews, **99**, 125-161.

663     Seneviratne SI, Lüthi D, Litschi M, Schär C (2006) Land–atmosphere coupling and climate

664           change in Europe. Nature, **443**, 205.

665     Shellito PJ, Small EE, Livneh B (2018) Controls on surface soil drying rates observed by

666           SMAP and simulated by the Noah land surface model. Hydrology and Earth System

667           Sciences, **22**, 1649-1663.

668     Short Gianotti DJ, Rigden AJ, Salvucci GD, Entekhabi D (2019) Satellite and station

669          observations demonstrate water availability's effect on continental-scale evaporative

670          and photosynthetic land surface dynamics. Water Resources Research, **55**, 540-554.

671     Stoy PC, El-Madany TS, Fisher JB *et al.* (2019) Reviews and syntheses: Turning the

672          challenges of partitioning ecosystem evaporation and transpiration into opportunities.

673          Biogeosciences, **16**, 3747-3775.

674     Teuling A, Seneviratne SI, Williams C, Troch P (2006) Observed timescales of

675          evapotranspiration response to soil moisture. Geophysical Research Letters, **33**.

676     Teuling AJ, Seneviratne SI, Stöckli R *et al.* (2010) Contrasting response of European forest

677          and grassland energy exchange to heatwaves. Nature Geoscience, **3**, 722.

678     Tramontana G, Jung M, Schwalm CR *et al.* (2016) Predicting carbon dioxide and energy

679          fluxes across global FLUXNET sites with regression algorithms.

680     Wang K, Dickinson RE (2012) A review of global terrestrial evapotranspiration: Observation,

681          modeling, climatology, and climatic variability. Reviews of Geophysics, **50**.

682     Zscheischler J, Orth R, Seneviratne SI (2015) A submonthly database for detecting changes in

683          vegetation-atmosphere coupling. Geophysical Research Letters, **42**, 9816-9824.

684

**Figure legends**

**Fig. 1** Schematic of the typical relationship between evaporative fraction (EF) and soil moisture (SM), as well as the changes in daily SM, gross primary production (GPP) and vapor pressure deficit (VPD) during soil moisture dry-down. We hypothesize that the covariance between daily VPD and GPP can be used to detect two regimes during dry-downs, i.e., one regime with energy limiting conditions (positive covariance) and one regime with water limiting conditions (negative covariance). "+" and "-" represent the positive and negative correlation, respectively. RAD: incoming shortwave radiation. During a SM dry-down, there is generally an initial period of GPP increase due to available SM after rainfall if the ecosystem is already water limited before the dry-down counting started.

**Fig. 2** EF-SM relationships for different vegetation types. Bold lines indicate binned median values calculated in equal SM bins of 1% increments, while shading bounds the 25th and 75th percentiles of EF values within soil moisture bins. EF: evaporative fraction; SM: soil moisture.

**Fig. 3** Probability density function of estimated critical soil moisture (SM) threshold (a) and soil matric potential threshold (b). Estimated SM threshold and soil matric potential threshold among different vegetation types (c). For each box plot, the middle line indicates the median; the box indicates the upper and lower quartiles and the whiskers indicate the 5th and 95th percentiles of the data. The numbers in brackets indicate the number of sites.

**Fig. 4** The evaporative fraction (EF) sensitivity to soil moisture (SM) (a), time fraction spent in water-limited stage (b) and the peak EF (c) among different vegetation types in Europe. For each box plot, the middle line indicates the median; the box indicates the upper and lower quartiles and the whiskers indicate the 5th and 95th percentiles of the data. The numbers in brackets indicate the number of sites.

**Fig. 5** Daily soil moisture (SM), gross primary production (GPP) and vapor pressure deficit (VPD) during a soil dry-down at CH-Cha (grassland, a). Covariance between daily VPD and GPP changes with moving windows (b), and evaporative fraction (EF) changes with SM during the dry-down (c). The unit of covariance is $\mu mol\ CO_2\ m^{-2}\ s^{-1}\ hPa$. The color coding in panel (c) indicate the soil moisture values. Please note that the soil moisture scale is from high to low.

**Fig. 6** Covariance between daily vapor pressure deficit (VPD) and gross primary production (GPP) across nine-day moving window changes with moving windows after rainfall during the dry-down (a-d). Mean soil moisture (SM) during moving window for each dry-down (e-h). Comparison between the critical SM thresholds estimated from the VPD-GPP covariance method and evaporative fraction (EF) method (i-j). Covariance and mean soil moisture were calculated using 9-day moving window (e.g., 1-9 days; 2-10 days; 3-11 days…). Each black line represents the covariance change at each dry-
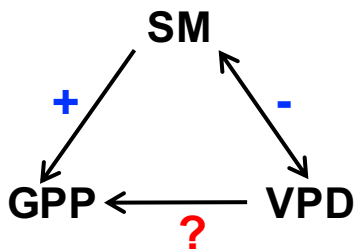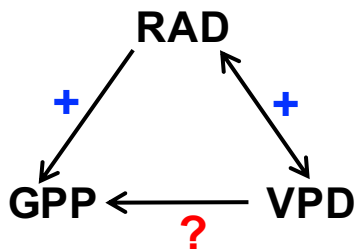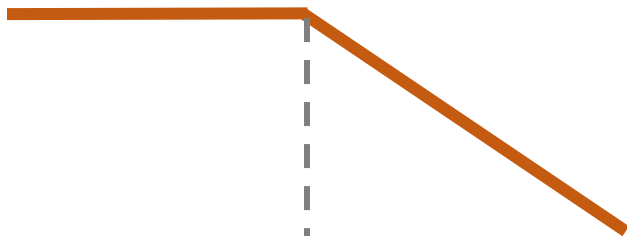
722   down while the red line means the median value in equal bins of 1 day change (a-d). The shading

723   bounds the 25th and 75th percentile of the distribution of covariance within the bin (a-d). The units of

724   covariance is μmol $CO_2$ m$^{-2}$ s$^{-1}$ hPa.

725

726   **Fig. 7** Relative importance of mean annual precipitation (MAP), clay fraction, summer average vapor

727   pressure deficit (VPD), incoming shortwave radiation (RAD) and wind speed to the spatial variability

728   of soil moisture (SM) thresholds (a) and evaporative fraction (EF) slopes (b).

| Energy-Limited | Water-Limited |

EF

RAD
$+$      $+$
GPP ← **?** VPD

SM
$+$      $-$
GPP ← **?** VPD

SM

GPP

VPD
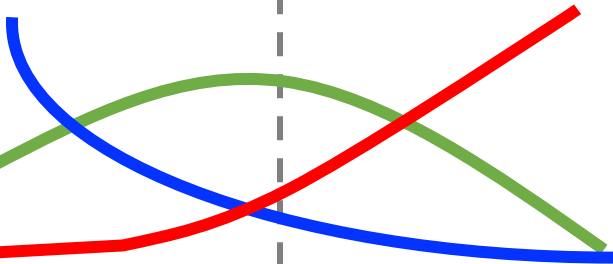
Progression in Time
During drydown

**(a)**

y-axis: ΔEF per SM decrease

x-axis categories: All (23), Boreal forests (3), Temperate forests (14), Temperate grasslands (2), Mediterranean savannas (3)

**(b)**

y-axis: Time spent in water-limted stage (%)

x-axis categories: All (23), Boreal forests (3), Temperate forests (14), Temperate grasslands (2), Mediterranean savannas (3)

**(c)**

y-axis: Peak EF

x-axis categories: All (23), Boreal forests (3), Temperate forests (14), Temperate grasslands (2), Mediterranean savannas (3)

**(a)** CH-Cha

**(a)**

Relative importance to the spatial variability of SM thresholds (%)

$R^2 = 0.74$

MAP, Clay, VPD, RAD, Wind

**(b)**

Relative importance to the spatial variability of EF slopes (%)

$R^2 = 0.65$

MAP, Clay, VPD, RAD, Wind